Two-state approach to stochastic hair bundle dynamics

Diana Clausznitzer,* Benjamin Lindner, and Frank Jülicher
Max-Planck-Institut für Physik Komplexer Systeme, Nöthnitzer Strasse 38, 01187 Dresden, Germany

Pascal Martin
Laboratoire Physico-Chimie Curie, Centre National de la Recherche Scientifique-Unit Mixte de Recherche 168, Institut Curie Recherche, 26 Rue d'Ulm, 75248 Paris Cedex 05, France

(Received 18 December 2007; published 1 April 2008)

Hair cells perform the mechanoelectrical transduction of sound signals in the auditory and vestibular systems of vertebrates. The part of the hair cell essential for this transduction is the so-called hair bundle. *In vitro* experiments on hair cells from the sacculus of the American bullfrog have shown that the hair bundle comprises active elements capable of producing periodic deflections like a relaxation oscillator. Recently, a continuous nonlinear stochastic model of the hair bundle motion [Nadrowski *et al.*, Proc. Natl. Acad. Sci. U.S.A. **101**, 12195 (2004)] has been shown to reproduce the experimental data in stochastic simulations faithfully. Here, we demonstrate that a binary filtering of the hair bundle's deflection (experimental data and continuous hair bundle model) does not change significantly the spectral statistics of the spontaneous as well as the periodically driven hair bundle motion. We map the continuous hair bundle model to the FitzHugh-Nagumo model of neural excitability and discuss the bifurcations between different regimes of the system in terms of the latter model. Linearizing the nullclines and assuming perfect time-scale separation between the variables we can map the FitzHugh-Nagumo system to a simple two-state model in which each of the states corresponds to the two possible values of the binary-filtered hair bundle trajectory. For the two-state model, analytical expressions for the power spectrum and the susceptibility can be calculated [Lindner and Schimansky-Geier, Phys. Rev. E **61**, 6103 (2000)] and show the same features as seen in the experimental data as well as in simulations of the continuous hair bundle model.

DOI: 10.1103/PhysRevE.77.041901 PACS number(s): 87.19.lt, 87.10.Mn, 02.50.Ey, 05.10.Gg

I. INTRODUCTION

The ear shows several remarkable features which are characteristic for an active system. It can detect stimuli that span several orders of magnitude in strength, while amplifying sounds near the hearing threshold and it can resolve small differences in frequency. Another surprising feature showing clearly the ear's activity is the *generation* of sound by the ear (otoacoustic emissions). The mechanism by which this activity mediates and enhances our perception of auditory stimuli in such a remarkable way is not clear at all. In all vertebrates one element of the signal transduction chain which is certainly involved in the activity mechanism is the hair cell of the inner ear [1].

The hair cell is responsible for mechanoelectrical transduction translating a mechanical stimulus into electrical signals that can be transmitted to the brain. On the top (or apical) side of the hair cell a distinct structure, the hair bundle, protrudes into the extracellular fluid which is composed of fingerlike elements, the so-called stereocilia. Mechanical stimuli are mediated to the hair bundle either via viscous drag forces from the surrounding fluid or direct deflection by an overlying membrane, which is attached to the hair bundle. A deflection of the bundle results in the opening of mechanically gated ion channels at the tips of the stereocilia giving rise to a transduction current which controls the release of a neurotransmitter at the bottom of the hair cell.

The mechanisms of the active process and the way hair cells are involved is still under debate. There is some evidence that hair bundle motility can play an important role. The hair bundle is capable of producing spontaneous oscillations which may be related to the aforementioned otoacoustic emissions. It was shown for hair bundles in the sacculus of the American bullfrog that their oscillations are due to an active mechanism [2]. Activity means here first of all that the hair bundle operates out of thermodynamical equilibrium. This was shown by comparing spectral properties of the spontaneous and the periodically driven hair bundle movement and demonstrating that the fluctuation-dissipation relation (a signature of any equilibrium system) was violated.

The hair bundle is capable of amplifying weak stimuli, and does so in a frequency-selective manner with the amplification being greatest around its characteristic frequency of spontaneous oscillations [3]. Further, the hair bundle shows a compressive nonlinearity of its response to stimuli of increasing amplitude [4]. This means that many of the remarkable features of auditory signal processing may originate in the nonlinear dynamics of hair cells.

It was proposed that frequency selectivity and nonlinear compression are signatures of a system operating close to an oscillatory instability, a Hopf bifurcation [4–6]. In [7] a stochastic model for hair bundle dynamics was put forward where an oscillatory instability occurs due to the interplay between the calcium-dependent activity of adaptation motors on the inside of stereocilia at the site of the transduction channel complex and a region of negative slope in their force-displacement relation. This hair bundle model shows,

*Present address: Division of Molecular Biosciences, Imperial College London, London, UK.

depending on the choice of two parameters, oscillations which reproduce the general shape of oscillations as seen in experiments as well as spectral features that describe the properties of the oscillation in their stochastic nature.

Here, we focus on yet another aspect, that is the resemblance of the spontaneous and the periodically driven motion of the hair bundle to relaxation oscillations. Experimental recordings show that the hair bundle during its oscillation remains for long periods of time around one of two distinct positions and exhibits swift switches between them. We therefore look at a system which involves the dynamics of two variables showing a pronounced time-scale separation and study its statistical properties.

In this paper we demonstrate that the binary filtering of experimental data does not alter the spectral properties drastically, but still captures their main features. We utilize an analytical approach to a two-state description for hair bundle dynamics that corresponds to the aforementioned binary filtering. Our starting point is a stochastic model for the hair bundle [7] comprising two dynamical variables. The mechanical deflection of the hair bundle is described in a continuous way, and this model is henceforth called the continuous hair bundle model. Simulations of this model have shown excellent agreement with experimental data using only two free parameters that allow for a number of bifurcations: from a monostable (possibly excitable) to a bistable and also oscillatory regime; the agreement with experimental data was best in the oscillatory regime. Recently, the same model has been successfully applied to model spontaneous oscillations and other manifestations of active hair-bundle motility in three different species [8].

We perform a mapping of the continuous hair bundle model to the well-known stochastic FitzHugh-Nagumo (FN) model [9]. Although mathematically completely equivalent to the original model, the FN model has several advantages: (i) the nonlinearity appears only in one of the dynamical equations; (ii) the distinction of a slow and a fast variable reflects in a simple way the observed relaxation-oscillator-like behavior; (iii) the bifurcations can be more easily visualized by well-known phase-plane techniques from nonlinear dynamics; and (iv) further simplifications (piecewise linearization of the system's nullclines and the assumption of perfect time-scale separation) permit the calculation of spectral measures. This latter point has been demonstrated in [10] and will be utilized in this paper. Note that a mapping of a continuous dynamical system to a solvable two-state system was performed also for other nonlinear systems [11].

In Fig. 1, one main result of this paper is summarized. Experimentally measured power spectrum and linear response function are shown in comparison to analytical curves according to our two-state theory. Regarding the two-state approach and the binary filtering of the hair bundle's dynamics an additional remark is indicated: The output signal of the hair bundle is not its mechanical motion but the transduction current that stimulates the cell's synapses and thus triggers neural signals to the brain. This transduction current is a sigmoidal function of the bundle's deflection, i.e., it just knows essentially the two states of the dynamics which we attempt to approximate in this paper. Hence the two-state description being only an approximation to the hair

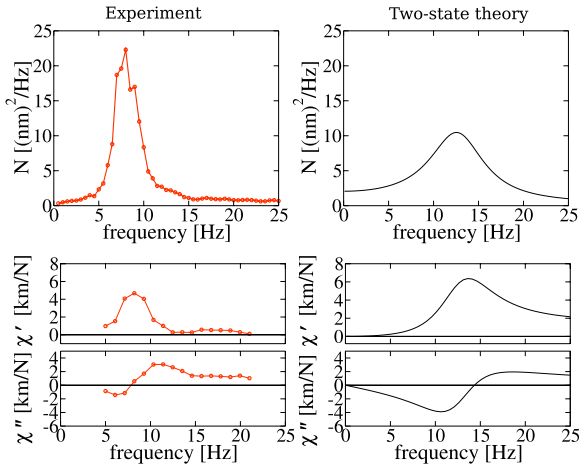

FIG. 1. (Color online) Comparison of experimentally measured spectrum and linear response function (binary-filtered data; left) and analytically obtained spectrum and susceptibility from the two-state model (right) for the hair bundle.

bundle's deflection may be a good model for the transduction current, i.e., for the actual output signal of the system.

The outline of our paper is as follows: In Sec. II the spectral quantities of interest are introduced and calculated for experimental data of spontaneous and stimulated hair bundle oscillations. Further, the influence of a binary filtering of the measured data on the spectral properties is investigated. In Sec. III, we briefly review the continuous hair bundle model from Ref. [7] and show simulation results for the spectral measures of the continuous and binary-filtered versions of the output of this model. In Sec. IV we introduce the exact mapping to a FitzHugh-Nagumo (FN) model, discuss the system's bifurcations (which are unchanged by the mapping) in terms of the nullclines of the FN model, and introduce a piecewise linear approximation of the nullclines. Based on the latter piecewise linear version of the FN dynamics and on the assumption of a perfect time-scale separation, we derive in Sec. V following Ref. [10] the two-state model. For this model, we calculate spectral quantities such as the power spectral density for the spontaneous activity, and the susceptibility for the driven dynamics in the limit of small stimulus amplitudes. Comparing to numerical simulation results of the continuous hair bundle model we demonstrate that the analytical two-state model captures the most important spectral features of the dynamics of the continuous model and of the experimental data. We summarize our results in Sec. VI and discuss directions of future work on the stochastic dynamics of hair bundles.

II. EXPERIMENTAL DATA

The sacculus is a vestibular organ in the inner ear involved in the detection of linear accelerations. Experimental raw data [2] obtained from hair cells of the sacculus of the bullfrog were reanalyzed. In those experiments the saccular macula was dissected from the frog and placed into a two-compartment chamber filled with two different fluids with

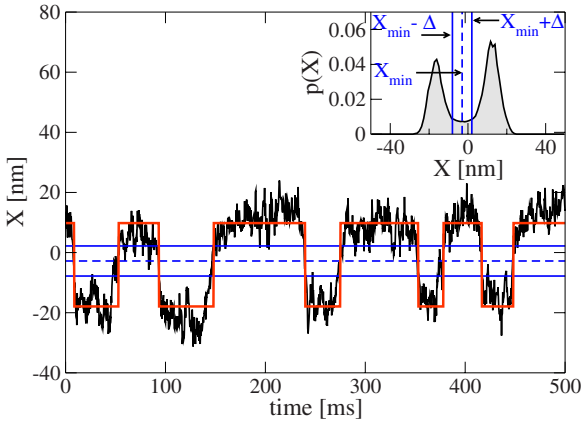

FIG. 2. (Color online) Binary-filtering of the hair bundle's trajectory. A sample trajectory $X(t)$ of a spontaneous hair bundle oscillation and its discretization is depicted. The inset shows the probability distribution $p(X)$ for spontaneous oscillations. In order to discretize the trajectory we implemented a two-threshold criterion where the trajectory has to cross a state-dependent threshold. The minimum X_{min} of the probability distribution for X serves as an indicator at which position X a transition occurs. There the trajectory spends the least time because it is fast and therefore the probability is reduced. The two thresholds are placed symmetrically about the minimum $X_{min} \pm \Delta$. The discretization procedure is then as follows: being in state σ_-, $X(t)$ needs to cross the threshold $X_{min}+\Delta$ to detect a transition. Being in state σ_+, the threshold is set to $X_{min}-\Delta$. We chose $\Delta=5$ nm throughout this paper. The discretization thresholds $X_{min} \pm \Delta$ are indicated in the figure. The peak-to-peak amplitude $\sigma_+-\sigma_-$ of the binary trajectory was adjusted such that the variances of the two processes are equal.

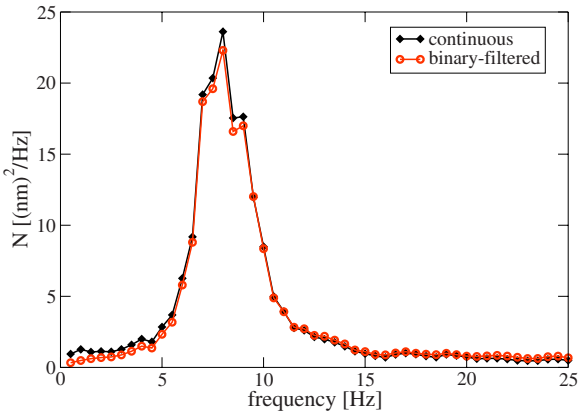

FIG. 3. (Color online) Power spectrum for experimentally measured (continuous) spontaneous oscillations and their binary-filtered version. The power spectrum was calculated for 16 trajectories which were averaged. Corresponding to the procedures in [2] the running average was performed over three data points, which is equivalent to a 1 Hz band.

ionic compositions resembling *in vivo* conditions. A flexible glass fiber was attached to the kinocilium of a single hair bundle in order to detect the hair bundle's position, X, as well as to stimulate it externally by moving the fiber's base. A detailed description of the experimental techniques can be found in [3].

When not excited by the glass fiber the bundle exhibited spontaneous oscillations. In a first experiment these were recorded. From these data the power spectral density was estimated in [2]. In a second experiment the hair bundle was stimulated by displacing the base of the fiber. A sinusoidal stimulus of different frequencies was applied for a duration of 50 cycles and the displacement of the hair bundle's tip was recorded. From those the linear response function was calculated in [2].

A. Discretization of the data

A sample trajectory of a spontaneous oscillation is displayed in Fig. 2 together with its discretization illustrating the binary filtering of the data. The hair bundle shows characteristic relaxation oscillations: it remains in the vicinity of one of two extreme positions for a long period of time and exhibits fast transitions between those positions. The two extreme positions will henceforth be called "σ_-" or "left state" (small X values) and "σ_+" or "right state" (high X value).

B. Power spectrum

The power spectral density, or short power spectrum, $N(f)$ is defined as the average of the absolute square of the Fourier transform of a trajectory $X(t)$ normalized by the recording time interval:

$$N(\omega) = \frac{\langle \tilde{X}\tilde{X}^* \rangle}{T_{int}}, \tag{1}$$

where the tilde denotes the Fourier transform $\tilde{X} = \int_0^{T_{int}} X(t) e^{i\omega t} dt$, the asterisk the complex conjugate, and $\langle \cdot \rangle$ is the ensemble average. T_{int} is the time interval of recording. The power spectrum for the spontaneously oscillating hair bundle was calculated and several smoothing procedures were applied as described in [2]. The power spectrum shows a peak at around 8 Hz meaning that this is the main frequency component in the oscillation. This frequency is called the characteristic frequency of the hair bundle. Further, the finite width of the peak indicates the fluctuation of frequency components around the characteristic frequency and therefore the finite phase coherence of the oscillation.

In Fig. 3 the power spectral densities for the continuous and binary-filtered data are shown. We observe a general quantitative agreement, especially around the characteristic frequency. Small differences appear at high frequencies, probably due to additional Fourier components that are introduced by the discretization, and at low frequencies where the spectral density for the discretized data is lower. This is probably due to neglecting the slow dynamics, and therefore excluding low frequencies, by the discretization.

C. Response to sinusoidal stimuli

Measuring the hair bundle mean deflection $\langle X \rangle$ in response to a sinusoidal external force $F(t)=F_0 \cos(\omega_s t)$ due to the displacement of the fiber's base the linear response function and its Fourier transform, the susceptibility, of the hair bundle can be calculated as derived in [2].

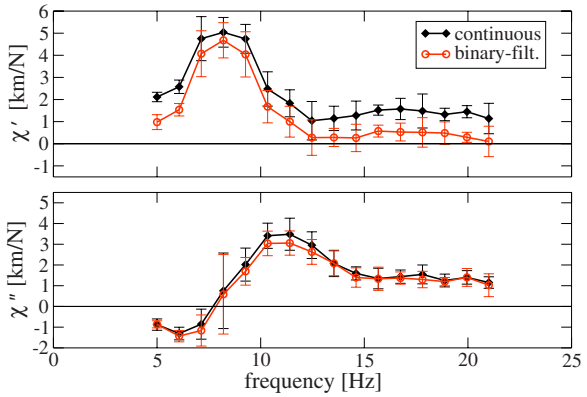

FIG. 4. (Color online) Real and imaginary part of the susceptibility of the periodically stimulated hair bundle for the continuous and binary-filtered trajectory. The error bars shown are the standard deviations determined by splitting the total time interval of stimulation into five parts.

The mean of the Fourier transform of the trajectory $X(t)$ with a weak stimulus $F(t)$ present defines the susceptibility by the following relation:

$$\langle \tilde{X}(\omega_s) \rangle = \chi(\omega_s)\tilde{F}(\omega_s) \tag{2}$$

From this relation one can easily determine the complex-valued susceptibility from an ensemble of measured trajectories and the corresponding input signals.

In Fig. 4 the susceptibility is shown for the continuous and discretized data. Again, agreement between both is good, and the main properties of this spectral statistics are reproduced quantitatively by the discretized data: The real part peaks at about the characteristic frequency leveling out to a plateau at higher frequencies. The imaginary part is negative for frequencies below the characteristic frequency. This is a manifestation of an active process, as in a passive (equilibrium) system the imaginary part is always positive. The modulus peaks near the characteristic frequency of the spontaneous oscillation yielding amplification most pronounced for this frequency (data not shown). A main difference between the susceptibility functions is apparent in the real part, where the linear response has a smaller amplitude for the binary-filtered data.

For the spectral quantities considered the agreement between the continuous and discretized data is striking. The main spectral properties in the hair bundle's oscillation are represented in the statistics of the switching between the two states. In the remainder of the paper we will use an analytical approach to a two-state description, for which one can calculate some spectral measures such as the power spectrum and the susceptibility analytically.

III. CONTINUOUS HAIR BUNDLE MODEL

The mechanical properties of hair bundle displacements can be described by a continuous model [7]. This description, which we refer to in the following by "continuous hair bundle model," is based on the gating spring model of mechanotransduction [12]. Deflections of the stereocilia, which all are assumed to act in parallel, induce tension in the gating springs. This tension subsequently triggers the opening of mechanosensitive ion channels. Adaptation motors, most likely myosin 1c, slide in response to mechanical stimulation to relax the tension in the gating spring. Finally, calcium ions which enter by the open transduction channels regulate the force generated by the adaptation motors and provide a negative feedback that is important for the generation of oscillations.

The continuous hair bundle model describes the dynamics of two displacement variables, the hair bundle deflection X and the displacements X_a of adaptation motors along the stereociliar axis projected on the X axis. These variables obey the dynamic equations

$$\lambda \dot{X} = -K_{GS}(X - X_a - DP_0) - K_{SP}X + F(t) + \eta_X(t), \tag{3}$$

$$\lambda_a \dot{X}_a = K_{GS}(X - X_a - DP_0) + F_{max}\left(S\frac{C}{C_M} - 1\right) + \eta_a(t) \tag{4}$$

in response to an externally applied force $F(t)$. Here, deflection of the hair bundle along the axis of mechanoelectrical sensitivity, i.e., perpendicular to the hair bundle's plane of bilateral symmetry, the variable X_a describes the position of molecular motors along the long axis of the stereocilium as projected onto the X axis described. The stereociliar pivot stiffness is denoted K_{SP}, the gating spring stiffness K_{GS}, and D denotes the displacement generated by the opening of channels. The open probability of transduction channels depends on the extension of gating springs, characterized by the difference $X - X_a$, as

$$P_0 = \frac{1}{1 + Ae^{-(X-X_a)K_{GS}D/k_BTN}}. \tag{5}$$

Here, $A = e^{[\Delta G + K_{GS}D^2/2N]/k_BT}$, where N is the number of ion channels, ΔG is the energy difference between the open and closed state of a channel, k_B denotes the Boltzmann constant, and T temperature. Opening of ion channels leads to a change in the intracellular calcium concentration $C = (C_M - C_0)P_0 + C_0 + \eta_C(t)$. Here, we assume that the relaxation time of the calcium concentration is fast compared to the other variables and C therefore changes instantaneously. For closed channels, C relaxes to the value C_0, while for open channels it reaches C_M in steady state.

The dynamic equation for the displacement X_a of the adaptation motors is based on a force velocity relationship $\lambda_a \dot{X}_a = F_{load} - F_{mot}$, where $F_{load} = K_{GS}(X - X_a - DP_0)$ is the gating force that acts as a load and F_{mot} is the maximal force the motor can generate. This maximal force is assumed to be regulated by the calcium concentration which to linear order can be expressed as $F_{mot} \simeq F_{max} + (\partial F_{mot}/\partial C)C$. The strength S of this feedback is defined by $S = -C_M(\partial F_{mot}/\partial C)$.

The bifurcation diagram of this system in the absence of noise and external forces is shown in Fig. 5. Depending on the control parameters F_{max} and S the hair bundle displays several dynamical regimes: an oscillatory regime (OSC in

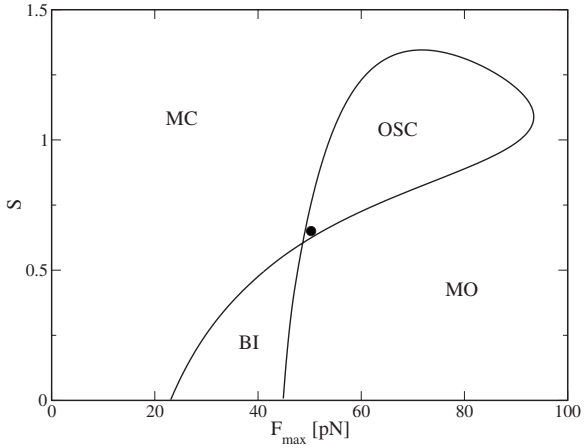

FIG. 5. Bifurcation diagram for the continuous hair bundle model equations (3) and (4) in the absence of noise and signal [i.e., $\eta_X(t) \equiv \eta_a(t) \equiv \eta_C(t) \equiv F(t) \equiv 0$]. The operation point of the hair bundle (point of best agreement of simulation with experimental data) is indicated by the black dot at $F_{max}=50.3$ pN, $S=0.65$.

Fig. 5), a bistable regime (BI), and two monostable regimes with high (MO) and low (MC) open probability of the transduction channels.

Finally noise terms η_X, η_a, and η_C have been added to describe the effects of fluctuations. These are Gaussian random variables with zero average and autocorrelations

$$\langle \eta_X(t)\,\eta_X(0)\rangle \equiv 2Q_X\delta(t) = 2k_BT\lambda\,\delta(t),$$

$$\langle \eta_a(t)\,\eta_a(0)\rangle \equiv 2Q_{X_a}\delta(t) = 2k_BT_a\lambda_a\delta(t),$$

$$\langle \eta_C(t)\,\eta_C(0)\rangle \equiv 2Q_C\delta(t) = 2C_M^2P_0(1-P_0)\tau_C/N\delta(t).$$

For noise strengths $T_a=1.5T$ and $\tau_C \simeq 1$ ms, this model agrees quantitatively with experiments for $F_{max}=50.3$ pN and $S=0.65$. The power spectrum and the susceptibility obtained by stochastic simulations of the model with these parameter values are shown in Figs. 6 and 7. The set (F_{max}, S) is located in the deterministically oscillatory region close to the boundary to bistable and monostable regimes (indicated as the operation point in Fig. 5). As for the experimental data in the previous section, we study the effects of binary filtering of the hair bundle's trajectory in the spontaneous case (power spectrum in Fig. 6) and the case of periodic driving (susceptibility in Fig. 7). The filtering procedure was the same as for the experimental data.

The power spectrum of the spontaneous activity does not change significantly upon binary filtering. Only slight differences appear at low and high frequencies similar to that seen for the experimental data. The main frequency (the characteristic frequency) between 8 and 9 Hz is well-reproduced by the continuous hair bundle model and the binary-filtered version.

If we switch on a periodic driving $F(t)=F_0\cos(\omega_s t)$ in the continuous hair bundle dynamics, the susceptibility (Fig. 7, diamonds) shows the same features as were seen in the experimental data (Fig. 4): its real part has a peak at about the

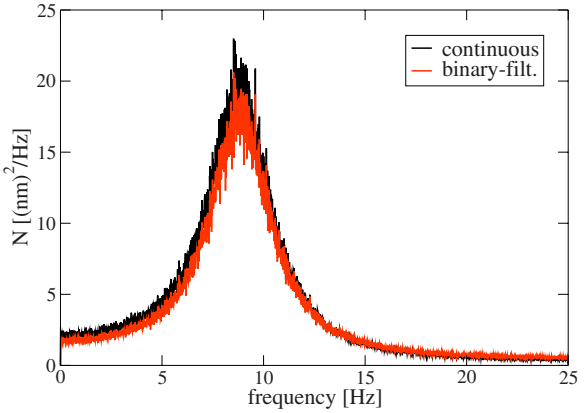

FIG. 6. (Color online) Power spectrum for the spontaneous activity of the continuous hair bundle model. Trajectories were simulated according to Eqs. (3) and (4) for $F_{max}=50.3$ pN and $S=0.65$ at the operation point of the hair bundle and binary filtered. The binary filtering was done as described for the experimental data. Compare to the experimentally measured spectra in Fig. 3.

characteristic frequency of the power spectrum. At about the same frequency the imaginary part of the susceptibility goes through zero. For smaller frequencies the imaginary part is negative. All of these features are captured by the binary-filtered version (circles) of the simulations. However, some small differences between the susceptibilities of the continuous dynamics and its binary version can be noticed: as for the experimental data the real part is slightly underestimated at all frequencies resulting in a zero crossing at high frequency of about 20 Hz (the zero crossing depends on the method of binary filtering and can be shifted to higher frequencies by adjusting the thresholds of discretization). Additionally, both the real and the imaginary parts go to zero for vanishing frequency—here the continuous response approaches a finite real value.

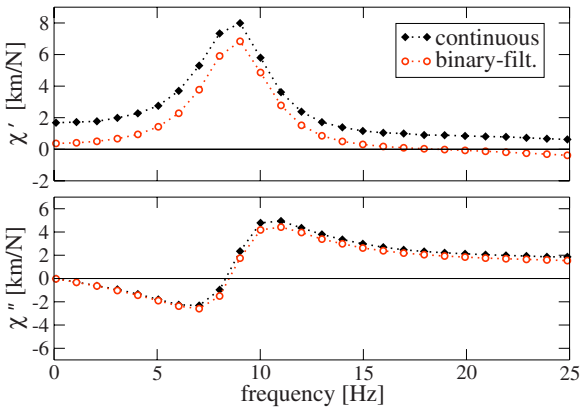

FIG. 7. (Color online) Real and imaginary part of the susceptibility of the continuous hair bundle model with respect to a sinusoidal force of amplitude 1 pN. Trajectories were simulated according to Eqs. (3) and (4) for $F_{max}=50.3$ pN and $S=0.65$ at the operation point of the hair bundle (diamonds) and binary filtered (circles). The binary filtering was done as described for the experimental data. Compare to the experimentally measured susceptibility in Fig. 4.

In summary, spectral features of the continuous hair bundle model (which reproduces well the experimental data) do not change upon binary filtering of its output. This gives additional motivation to aim at a two-state description of the hair bundle dynamics.

IV. TRANSFORMATION OF HAIR BUNDLE MODEL TO A FITZHUGH-NAGUMO MODEL

The relaxation oscillator nature of the hair bundle Eqs. (3) and (4) is revealed when the dynamical variables are linearly transformed. We introduce new dimensionless variables x and y that are linear combinations of the dynamical variables X and X_a with

$$x = \frac{1 - \alpha\beta + \frac{K_{SP}}{K_{GS}}(1-\alpha)^2}{D(1-\alpha\beta)^2}(X - X_a), \tag{6}$$

$$y = \frac{K_{SP}}{DK_{GS}}\frac{1-\alpha}{1-\alpha\beta}\left(X - \frac{1-\alpha}{1-\alpha\beta}(X - X_a) - \frac{F_{max}}{K_{SP}}\frac{\alpha}{1-\alpha}\right), \tag{7}$$

where α and β are dimensionless parameters

$$\alpha = \frac{\lambda}{\lambda + \lambda_a}, \tag{8}$$

$$\beta = \frac{F_{max}S}{DK_{GS}}. \tag{9}$$

By this transformation the new variables x and y satisfy a system of two differential equations that resembles a FitzHugh-Nagumo (FN) system:

$$\tau_x \dot{x} = f(x) - y + s_x(t), \tag{10}$$

$$\tau_y \dot{y} = Bx - y + y_0 + s_y(t). \tag{11}$$

For the cases considered here, the nonlinear function

$$f(x) = \frac{1}{1 + A\exp(-x/\delta)} - x \tag{12}$$

is shaped like an inverted N as it is typical for a FN system. The remaining parameters are given by

$$\tau_x = \frac{\alpha\lambda_a/K_{GS}}{1 + \frac{K_{SP}}{K_{GS}}\frac{(1-\alpha)^2}{1-\alpha\beta}}, \quad \tau_y = \frac{\lambda}{\alpha K_{SP}}\frac{1-\alpha\beta}{1-\beta}, \tag{13}$$

$$B = \frac{1}{1 + \frac{(1-\alpha)^2}{1-\alpha\beta}\frac{K_{SP}}{K_{GS}}}\frac{1-\alpha\beta}{1-\beta} - 1, \quad y_0 = -\frac{\beta}{S(1-\beta)},$$

$$\delta = \frac{k_B TN}{K_{GS}D}\frac{1 + \frac{K_{SP}}{K_{GS}}\frac{(1-\alpha)^2}{1-\alpha\beta}}{D(1-\alpha\beta)}. \tag{14}$$

The time-dependent terms $s_x(t) = \frac{1}{DK_{GS}}\frac{1-\alpha}{1-\alpha\beta}F(t) + \eta_x(t)$ and $s_y(t) = \frac{1}{DK_{GS}}\frac{1-\alpha}{1-\alpha\beta}F(t) + \eta_y(t)$ contain the external forcing as well as noise terms. The noise sources η_x and η_y are correlated; they contain linear combinations of the three uncorrelated noise sources $\eta_X(t)$, $\eta_a(t)$, and $\eta_C(t)$:

$$\eta_x = \frac{1}{DK_{GS}}\left(\frac{1-\alpha}{1-\alpha\beta}\eta_X(t) - \frac{\alpha}{1-\alpha\beta}\eta_a(t)\right) \tag{15}$$

$$- \frac{\alpha\beta}{C_M(1-\alpha\beta)}\eta_C(t), \tag{16}$$

$$\eta_y = \frac{1-\alpha}{1-\alpha\beta}\left(\frac{1}{DK_{GS}}\eta_X(t) + \frac{1}{DK_{GS}}\frac{1}{1-\beta}\eta_a(t) + \frac{\beta}{(1-\beta)C_M}\eta_C(t)\right). \tag{17}$$

We can cast all time-dependent terms in the slow dynamics of y via a further linear, time-dependent transformation $\bar{y} = y - s_x(t)$ which transforms Eqs. (10) and (11) to

$$\tau_x \dot{x} = f(x) - \bar{y}, \tag{18}$$

$$\tau_y \dot{\bar{y}} = \tau_y \dot{y} - \tau_y \dot{s}_x = Bx - \bar{y} + y_0 + s_y(t) - s_x(t) - \tau_y \dot{s}_x(t). \tag{19}$$

Note that in the absence of explicitly time-dependent terms $\bar{y} = y$. In the following, we neglect the time derivative of the noise η_x.

A. Nullcline picture of the deterministic FitzHugh-Nagumo system

In the absence of an external stimulus and noise, the dynamical behavior of the system can be illustrated by plotting the nullclines, namely those lines in the phase plane where $\dot{x} = 0$ and $\dot{\bar{y}} = 0$, cf. Fig. 8.

The nullcline for the variable x (dashed lines in Fig. 8) is the nonlinear function $f(x)$. It consists of two outer branches, which are termed dynamically stable (attractive), and one inner branch, which is termed unstable (repulsive), with respect to x. The y nullcline (dashed-dotted lines in Fig. 8) is a straight line.

The system shows monostable, bistable, or oscillatory behavior, depending on the number and stability of fixed points (intersections of the two nullclines). Figure 8 visualizes four different situations in the phase plane and shows the two nullclines together with sample trajectories. Fixed points on the outer branches are stable [cf., Figs. 8(a) and 8(d)]: after a transient phase the trajectory runs into the fixed point. If the fixed point lies near the minimum or maximum point of the nonlinear nullcline but still on the outer branch, the system is stable and shows excitable behavior with respect to external forcing or noise. Fixed points on the outer left branch correspond to the case of low open probability [most channels closed, MC, cf. Fig. 8(a)], fixed points on the right branch to high open probability [most channels open, MO, cf. Fig. 8(d)].

Fixed points on the middle branch of the nonlinear nullcline are typically unstable. If the unstable fixed point is

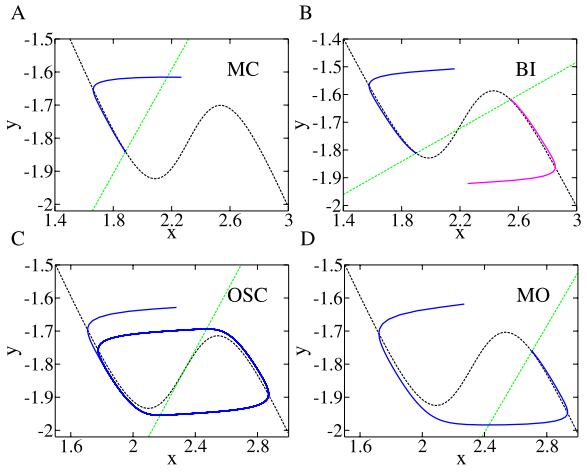

FIG. 8. (Color online) Nullclines (dashed and dashed-dotted lines) and deterministic sample trajectories (solid lines) for different parameters of F_{max} and S and for different initial conditions. (a) Monostable closed (MC, F_{max}=45.7 pN, S=0.7), (b) bistable (BI, F_{max}=47.1 pN, S=0.55; here two different initial conditions lead to different final states), (c) oscillatory (OSC, F_{max}=50.3 pN, S =0.65), and (d) monostable open (MO, F_{max}=53.6 pN, S=0.6).

the only one, the system is oscillatory and runs on a limit cycle close to the x nullcline [Fig. 8(c)]. If there are additional fixed points on the outer branches the system is bistable [Fig. 8(b)]. The parameter set chosen in Fig. 8(c) was found to match experimental data quantitatively in the presence of noise and corresponds to the operation point of the hair bundle. The other parameters lie in the vicinity of the operation point in the parameter plane and might be accessible by external or internal changes of the system parameters.

In all graphs in Fig. 8 a pronounced time-scale separation between x and y is visible: the x dynamics relaxes very fast, and therefore is always near the nullcline ($\dot{x}$=0) along the stable branches, and switches almost horizontally across the middle branch in the phase plane. The ratio τ_x/τ_y of the two time scales in Eqs. (10) and (11) describes the time-scale separation between the dynamics of x and y. For the operation point of hair bundle this ratio is of the order of 0.03, and therefore the x dynamics is fast compared to the y dynamics [16].

B. Piecewise linearization

We introduce a piecewise linear function $g(x)$ approximating $f(x)$ in Eq. (18), cf. Fig. 9. Both functions have the same nonlinear behavior, but $g(x)$ permits analytical calculations. The dynamical equations for x and $\bar{y}$ are replaced by

$$\tau_x \dot{x} = g(x) - \bar{y}, \tag{20}$$

$$\tau_y \dot{\bar{y}} = Bx - \bar{y} + y_0 + s_y(t) - s_x(t) - \tau_y \dot{s}_x(t). \tag{21}$$

Different choices of $g(x)$ can be used. The local minimum point $[x_m, y_m = f(x_m)]$ and the maximum point $[x_M, y_M = f(x_M)]$ of $f(x)$, respectively, are crucial for the dynamics of

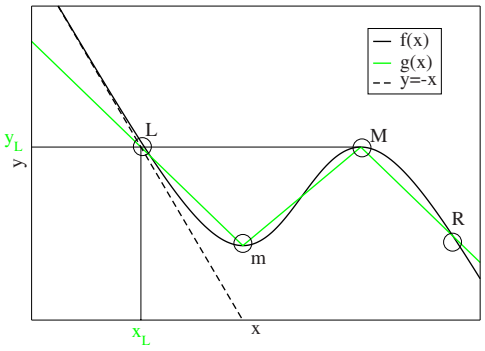

FIG. 9. (Color online) The x nullcline $f(x)$ is approximated by the piecewise linear function $g(x)$. The left branch of $g(x)$ is constructed by a line through the points L and m. L is the point on f on the left branch where the function attains the local maximum value y_M, i.e., $f(x_L)=y_M$ with $x_L<x_M$. In order to obtain an explicit expression for this point we neglect the nonlinear part of $f(x)$, which we assume to be small in this region. This leads to the condition $f(x_L)\approx -x_L$, i.e., $x_L \approx -y_M$. An equivalent reasoning yields the linear function for the right branch of g, which is defined as a line through M and R, where the point R is determined as $(x_R \approx y_m - 1, y_m)$. The middle branch is determined by a line through m and M, the minimum and maximum point of f.

the system. Hence we impose the condition that $g(x)$ has the same local minimum and maximum point. The function $g(x)$ is defined as

$$g(x) = \begin{cases} a_l x + b_l & \text{for } x < x_m, \\ a_c x + b_c & \text{for } x_m < x < x_M, \\ a_l x + b_r & \text{for } x > x_M. \end{cases} \tag{22}$$

The slopes of the two outer branches of $g(x)$ are equal such that $g(x)$ shares the same symmetry with the function $f(x)$. The positions x_m and x_M depend on the parameters A and δ of the nonlinear function $f(x)$ Eq. (12)

$$x_m = \delta \ln A - \delta \ln\left(\frac{1}{2\delta}\left(1 + \sqrt{1 - 4\delta}\right) - 1\right), \tag{23}$$

$$x_M = \delta \ln A - \delta \ln\left(\frac{1}{2\delta}\left(1 - \sqrt{1 - 4\delta}\right) - 1\right). \tag{24}$$

The construction of the linearization $g(x)$ is visualized in Fig. 9. The expressions for the slope and additive constants in Eq. (22) are

$$a_l = \frac{y_m - y_M}{x_m + x_M} = a_r, \quad b_l = y_m - \frac{y_m - y_M}{x_m + y_M}, \tag{25}$$

$$b_r = y_M - \frac{y_m - y_M}{1 - y_m + x_M}, \tag{26}$$

$$a_c = \frac{y_M - y_m}{x_M - x_m}, \quad b_c = y_m - \frac{y_M - y_m}{x_M - x_m} x_m. \tag{27}$$

V. ANALYTICAL TWO-STATE MODEL FOR THE HAIR BUNDLE

A. Mapping of the FitzHugh-Nagumo model to a two-state system

Following [10] we now set the short time-scale to zero,

$$\tau_x = 0. \tag{28}$$

This condition implies that the dynamics of x is enslaved by the slow dynamics of $\bar{y}$; at any instant in time the dynamics of x relaxes to its stationary value for a given $\bar{y}$. From Eq. (20), we see that x is determined by $g^{-1}(\bar{y})$. On the middle branch of g the dynamics is unstable, and therefore x assumes values on the two outer branches only. Put differently, the switching between the two outer branches becomes infinitely fast in the limit $\tau_x=0$.

We can now write down a very simple set of equations that determine the dynamics on the left and right branch:

$$\dot{u} = -u + s(t) + \eta(t), \tag{29}$$

$$\dot{v} = -v - s(t) + \eta(t). \tag{30}$$

Here, we have performed a linear transformation of the system time $t \to (1-\frac{B}{a_l})/\tau_y t$. The new variables $u=\bar{y}-(y_0 - \frac{Bb_l}{a_l})/(1-\frac{B}{a_l})$ and $v=-\bar{y}+(y_0-\frac{Bb_r}{a_l})/(1-\frac{B}{a_l})$ determine the dynamics on the left and right branch, respectively. We again consider a periodic forcing $F(t)$ for the hair bundle system. Therefore the deterministic external signal $s(t)$ reads

$$s(t) = \frac{\bar{\omega}_s F_0}{DK_{GS}} \frac{1-\alpha}{1-\alpha\beta} \sin(\bar{\omega}_s t). \tag{31}$$

Due to the transformation of the system's time the driving frequency is rescaled according to $\bar{\omega}_s = \omega_s \tau_y (1-\frac{B}{a_l})$. The noise η has zero mean and the autocorrelation

$$\begin{aligned}\langle \eta(t)\eta(t')\rangle &= \left(\left[\frac{\sqrt{2Q_{X_a}}}{DK_{GS}(1-\beta)} \right]^2 + \left[\frac{\beta\sqrt{2Q_C}}{C_M(1-\beta)} \right]^2 \right) \\ &\times \left| \frac{1}{\tau_y\left(1-\frac{B}{a_l}\right)} \right| \delta(t-t') \\ &\equiv 2Q\delta(t-t'),\end{aligned} \tag{32}$$

where we defined the noise intensity Q of η.

The dynamics on the two branches are connected via the boundary conditions. Whenever the trajectory hits the absorption point on one branch it switches to the other branch and is injected in the injection point. The absorption and injection points corresponding to the left branch are

$$u_- = g(x_m) - \frac{y_0 - \frac{Bb_l}{a_l}}{1-\frac{B}{a_l}}, \quad u_+ = g(x_M) - \frac{y_0 - \frac{Bb_l}{a_l}}{1-\frac{B}{a_l}} \tag{33}$$

and to the right branch

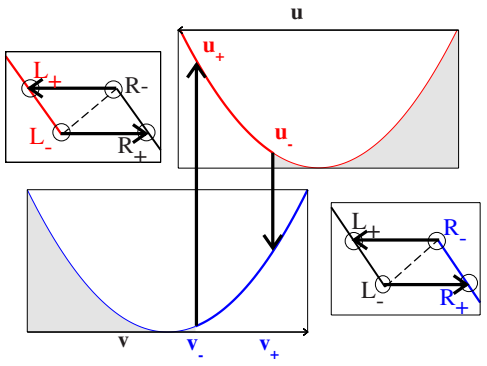

FIG. 10. (Color online) Two-state model: parabolic potentials with absorption and injection points exemplified for the oscillatory case. The branch of the piecewise linear FN nullcline for the dynamics of x are shown next to the corresponding parabolic potential. In the top (lower) panel the left (right) branch is depicted; the minimum (maximum) point L_- (R_-) of the nullcline corresponds to the absorption point u_- (v_-) of the dynamics in the parabolic potential, the point L_+ (R_+) corresponds to the injection point u_+ (v_+). In the absence of an external stimulus, Eqs. (29) and (30) describe diffusion in the parabolic potentials $\frac{1}{2}u^2$ and $\frac{1}{2}v^2$. In this intuitive picture, stable fixed points correspond to the minima of the parabolic potentials, i.e., $u=0$ or $v=0$. If there is no fixed point on a branch the potential minimum lies outside the interval defined by the injection and absorption point and the trajectory just "slides down" from the injection to absorption point.

$$v_- = -g(x_M) + \frac{y_0 - \frac{Bb_r}{a_l}}{1-\frac{B}{a_l}}, \quad v_+ = -g(x_M) + \frac{y_0 - \frac{Bb_r}{a_l}}{1-\frac{B}{a_l}}. \tag{34}$$

In the absence of an external stimulus there is an intuitive picture for the dynamics equations (29) and (30); the Langevin equations describe diffusion in parabolic potentials. Those potentials are sketched and absorption and injection points on each of the branches are indicated for the oscillatory case of the hair bundle model in Fig. 10. In the presence of an external stimulus the potential is modulated with time. For the system with noise equations (29) and (30) the corresponding Fokker-Planck equations can be solved for the stationary densities in each of the states, as well as for their characteristic functions of the residence times on each of the two branches [10].

We consider the binary process $\sigma(t)$: we assign the discrete values σ_+ and σ_- according to the occupation of the right or the left branch, respectively, and we obtain a two-state description for the FitzHugh-Nagumo model. For this process the power spectrum and susceptibility have been calculated [10].

B. Bifurcation diagram

Considering the deterministic case without noise or external signals, bifurcation analysis reveals that the two-state model exhibits different dynamical behavior in certain re-

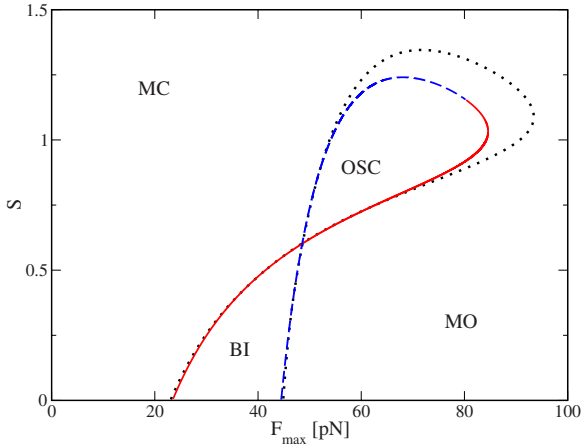

FIG. 11. (Color online) Bifurcation diagram for the continuous hair bundle model (dotted line) and the two-state system. The solid line is for the bifurcations through the intersection of the linear nullcline at the local maximum of $g(x)$, Eq. (A2), and the dashed line for bifurcations through the intersection at the minimum of $g(x)$, Eq. (A1). The intersection of the solid and the dashed lines mark the parameter values where $B=a_c$.

gimes of the parameters F_{max} and S. A bifurcation occurs when the y nullcline intersects the piecewise linear nullcline $g(x)$ at the local minimum point or the maximum point. Depending on the slope a_c of g on the middle branch and the slope B of the y nullcline the bifurcation is from monostable to oscillatory or bistable, respectively. For $B>a_c$ the stable fixed point on the outer branch is transformed into one unstable fixed point on the middle branch, or vice versa. If $B<a_c$, the stable fixed point branches at the bifurcation into an unstable fixed point on the middle branch, and two new stable fixed points on the outer branches, or vice versa.

The calculation of the bifurcation lines is shown in Appendix A, and the bifurcation diagram is depicted in Fig. 11. The comparison with the bifurcation diagram of the full system shows that both are in good agreement except for high motor forces at strong calcium feedback, where in the linearized model the solution is quiescent, but the full model still shows oscillations. In this regime, the nonlinear function $f(x)$ loses its pronounced local minimum and maximum. This means the distinction between different states loses its meaning and a two-state description is not appropriate.

C. Power spectrum

For the binary process $\sigma(t)$ that is governed by the dynamics equations (29) and (30) with boundary conditions (33) and (34) the power spectral density $N(\omega)$ has been calculated [10]. The spectrum is expressed in terms of the Fourier transforms of the probability distributions of the residence time in the left and right state $\sigma=\sigma_-$ and $\sigma=\sigma_+$, $w_l(\omega)$ and $w_r(\omega)$ [13],

$$N(\omega) = \frac{2r_0(\sigma_+ - \sigma_-)^2}{\omega^2} \mathrm{Re}\left(\frac{[1-w_l(\omega)][1-w_r(\omega)]}{1-w_l(\omega)w_r(\omega)}\right), \tag{35}$$

where r_0 is the inverse mean time for switching back and forth $\sigma_- \to \sigma_+ \to \sigma_-$ in the absence of an external signal

$$r_0^{-1} = \sqrt{\pi}\left[\int_{u_-/\sqrt{2Q}}^{u_+/\sqrt{2Q}} dz e^{z^2}\,\mathrm{erfc}(z) + \int_{v_-/\sqrt{2Q}}^{v_+/\sqrt{2Q}} dz e^{z^2}\,\mathrm{erfc}(z)\right], \tag{36}$$

with erfc$(\cdot)$ denoting the complementary error function. The characteristic functions are given as ratios of parabolic cylinder functions $\mathcal{D}_{i\omega}(x)$ [14],

$$w_l(\omega) = e^{\Delta_l}\frac{\mathcal{D}_{i\omega}(u_+/\sqrt{Q})}{\mathcal{D}_{i\omega}(u_-/\sqrt{Q})}, \tag{37}$$

$$w_r(\omega) = e^{\Delta_r}\frac{\mathcal{D}_{i\omega}(v_+/\sqrt{Q})}{\mathcal{D}_{i\omega}(v_-/\sqrt{Q})}, \tag{38}$$

where $\Delta_l=(u_+^2-u_-^2)/(4Q)$ and $\Delta_r=(v_+^2-v_-^2)/(4Q)$.

We show the power spectra of the spontaneous activity of the two-state model and the continuous model for the hair bundle for different parameters of F_{max} and S in Fig. 12. These correspond to the same parameter sets used to illustrate the different deterministic dynamical regimes of the hair bundle model by means of the FN system in Fig. 8. We find a peak in the power spectrum not only for the parameter set in the deterministically oscillatory regime ["OSC," cf. Fig. 12(c)], but also if the deterministic dynamics is in the bistable or one of the excitable regimes. This is a signature of noise-induced coherence [9]. The peak is most pronounced in the deterministically oscillatory case and broader for the deterministically stable systems. The characteristic frequency of the oscillation in the deterministically stable regimes is lower than in the oscillatory case. The two-state theory captures these features of the spectrum.

One main quantitative difference between the two-state theory and the continuous model is a shift of the main oscillation frequency to a higher frequency which is mainly due to the approximation of a perfect time-scale separation between the slow and the fast variable of the FN system by setting $\tau_x=0$. According to Eqs. (13) the ratio of the time-scale separation τ_x/τ_y depends only on the product of parameters $F_{max}S$. We can quantify the shift of the oscillation frequency by scanning through the parameter plane measuring at what frequency the spectra of the respective dynamics peak (cf. Figs. 13 and 14). As this shift depends critically on the value of the time-scale separation of the two dynamical variables, we expect that for a constant time-scale separation τ_x/τ_y the frequency shift is roughly constant. Figure 13 shows the characteristic frequency of the two-state model and the continuous hair bundle model scanning through the bifurcation diagram as indicated, leaving $F_{max}S=32.7$ pN constant. The peak frequency for the two-state theory is consistently higher than for the continuous hair bundle model by a factor of about 1.4. Walking on a line where P_0 is constant on the contrary changes the time-scale separation ratio τ_x/τ_y as well as the parameter B. Figure 14 depicts the characteristic frequency of the two-state model and the continuous hair bundle model for a scan through the bifurcation diagram along $P_0=0.5$. The ratio of the characteristic frequency of the approximation and the characteristic frequency increases

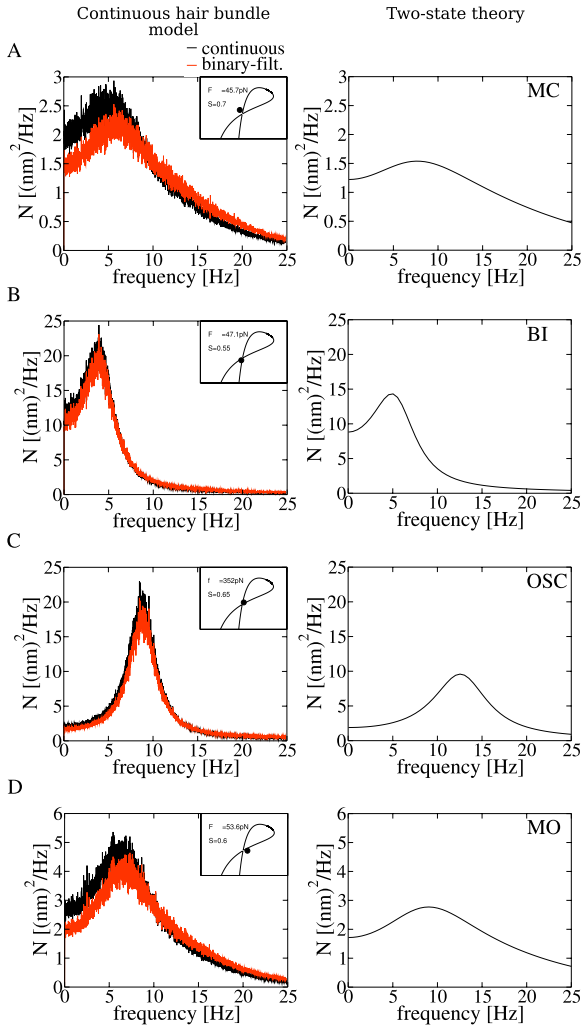

FIG. 12. (Color online) Power spectrum for the spontaneous dynamics. Left column: power spectra for X for simulations of the continuous hair bundle model and for its binary-filtered version, right column: power spectra for the analytical two-state approximation. The parameter sets correspond to the ones shown before and different dynamical regimes: (a) monostable closed (MC, F_{max} =45.7 pN, S=0.7), (b) bistable (BI, F_{max}=47.1 pN, S=0.55, (c) oscillatory (OSC, F_{max}=50.3 pN, S=0.65), and (d) monostable open (MO, F_{max}=53.6 pN, S=0.6). The peak-to-peak amplitude $\sigma_+ - \sigma_-$ of the binary processes was adjusted such that their variances are equal to the respective variance of the continuous process as measured by the integral over the power spectra.

with F_{max}, i.e., with diminishing time-scale separation and increasing B. The rescaling of the frequency will be discussed in detail in Sec. VI B.

D. Response to sinusoidal stimuli

In the presence of a small periodic stimulus $F(t)$ the system's spontaneous dynamics is expected to change. If the stimulus is small enough we expect that only the response at the driving frequency ω_s is affected. The susceptibility for the two-state system was calculated in [10] which for our system yields

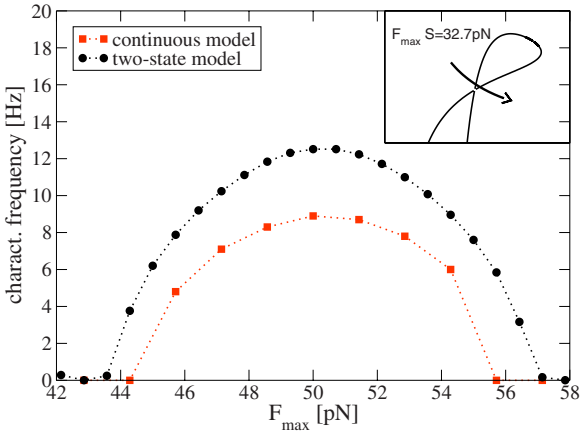

FIG. 13. (Color online) Shift of the characteristic frequency of the power spectrum varying F_{max} but leaving the time-scale separation τ_x/τ_y=0.029 (and $F_{max}S$=32.7 pN) constant. The peak frequency in the two-state theory (circles) is higher than in the continuous hair bundle model (squares) by a factor of about 1.4.

$$\chi(\bar{\omega}_s) = \frac{r_0(1-\alpha)}{DK_{GS}\sqrt{Q}(1-\alpha\beta)} \frac{i\bar{\omega}_s}{1-\bar{\omega}_s}(\sigma_+ - \sigma_-) \times \frac{(V_0^+ - V_0^-)(U_1^+ - U_1^-) + (V_1^+ - V_1^-)(U_0^+ - U_0^-)}{U_0^+ V_0^+ - U_0^- V_0^-}, \tag{39}$$

where we for brevity introduced the symbols $U_n^{\pm} = e^{u_{\pm}^2/(4Q)}\mathcal{D}_{i\bar{\omega}_s - n}(u_{\pm}/\sqrt{Q})$ and $V_n^{\pm} = e^{v_{\pm}^2/(4Q)}\mathcal{D}_{i\bar{\omega}_s - n}(v_{\pm}/\sqrt{Q})$. The susceptibilities for the hair bundle driven by a sinusoidal force are shown in Fig. 15 for the two-state theory and simulations of the continuous model for the hair bundle. The same parameter sets were used as discussed before for the power spectrum. For stochastic oscillatory dynamics of the hair bundle model the general features of the susceptibility

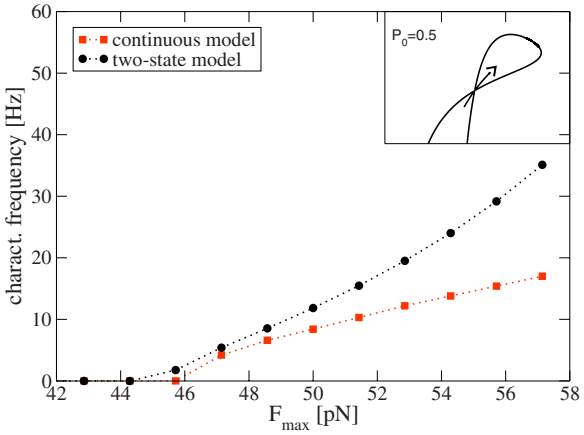

FIG. 14. (Color online) Shift of the characteristic frequency of the power spectrum varying F_{max} but leaving the open probability of the stationary state P_0=0.5 constant. The peak frequency in the two-state theory (circles) increases steeper compared to the continuous hair bundle model (squares).

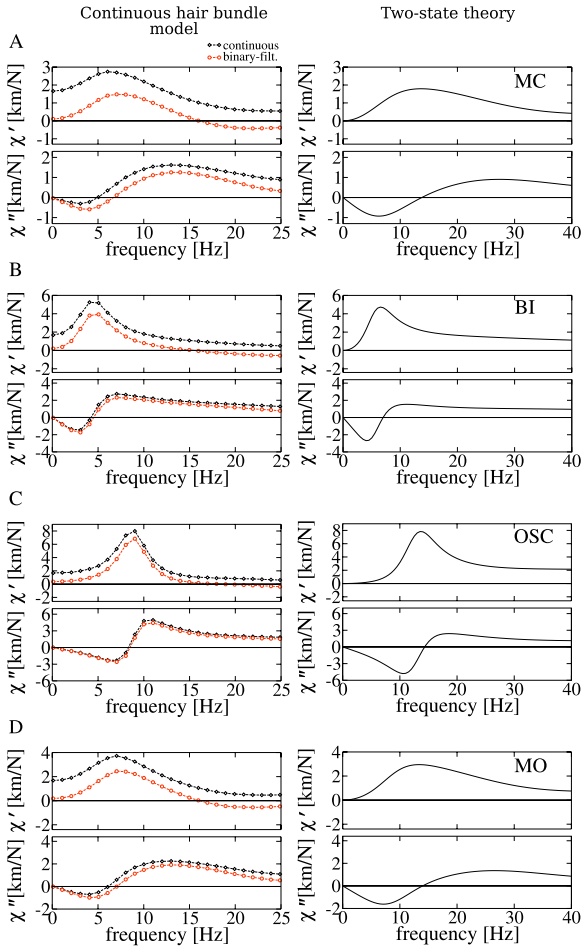

FIG. 15. (Color online) Real and imaginary part of the susceptibility of the periodically driven dynamics. Left column: susceptibility for simulations of the continuous hair bundle model with a sinusoidal force of amplitude 1 pN (diamonds) and of its binary-filtered version (circles), right column: susceptibility for the analytical two-state theory. The parameter sets correspond to the ones shown before and different dynamical regimes: (a) monostable closed (MC, F_{max}=45.7 pN, S=0.7), (b) bistable (BI, F_{max} =47.1 pN, S=0.55, (c) oscillatory (OSC, F_{max}=50.3 pN, S=0.65), and (d) monostable open (MO, F_{max}=53.6 pN, S=0.6). The peak-to-peak amplitude $\sigma_+ - \sigma_-$ of the binary processes was adjusted such that their variances are equal to the respective variance of the continuous process as measured by the integral over the power spectra. Note the different scaling of the frequency axes.

are the following: The real part of the susceptibility peaks at about the characteristic frequency of the power spectrum. At about the same frequency the imaginary part goes through zero. For smaller frequencies the imaginary part is negative. These characteristics are found more pronounced as parameters are chosen in the vicinity of the deterministic oscillatory regime. The two-state theory reproduces those features of the susceptibility as shown for the four parameter sets in Fig. 15.

As in the binary-filtered version of the simulated continuous model, the real and imaginary part of the analytical susceptibilities tend to zero for low frequencies. The real part of the analytical results of the two-state theory for the susceptibility is always positive and does not show a zero. This is a qualitative difference to the binary-filtered dynamics of the continuous hair bundle model. Furthermore, the maximum of the imaginary part compared to the minimum appears less pronounced in the two-state theory than in the continuous hair bundle model.

Also in the susceptibility the spectral features are shifted to a higher frequency, which we already saw for the power spectra. We will discuss a possible rescaling of spectral features in the discussion Section VI B for the operation point of the hair bundle.

VI. DISCUSSION AND OUTLOOK

In this paper, we investigated a binary description of the hair bundle's dynamics. First of all, we examined whether a binary filtering of hair bundle data (experiment and continuous model) changes the spectral statistics significantly. This is not the case, only minor changes were found—a binary description in terms of two discrete states can account for most of the observed spectral features. Motivated by this observation, we then developed an approximate mapping of the continuous dynamics onto a two-state system corresponding to the two discrete states of the binary description. In the following, we discuss the limitations of a binary description. Finally, we give an outlook on further applications of the two-state model.

A. Differences between the continuous and binary-filtered data

The binary description captures the main spectral statistics of the active hair bundle dynamics. The power spectrum of the binary variable showed a pronounced peak around 8 Hz, the real part of the susceptibility as well, and the imaginary part of the susceptibility was negative below and positive above this frequency of 8 Hz. Deviations between the spectral measures of the continuous and binary data were seen mainly in the real part of the susceptibility, similar in the simulation data as well as in the experimental data. This difference can be understood by an additive passive continuous dynamics as we will show now.

We decompose the deflection of the hair bundle to be a superposition $X(t)=\sigma(t)+\hat{X}(t)$ of the binary variable $\sigma(t)$ and a variable governed approximately by a linear equation $\lambda\dot{\hat{X}} = -K_{SP}\hat{X}+F(t)+\eta_X(t)$. Such a description is indeed valid in the limit of small driving frequency (i.e., in the case of a static stimulus) and is expected to reproduce the correct linear response for high frequencies, too.

Assuming that these two variables are statistically independent, one obtains for the response function of $X(t)$

$$\chi_X(\omega) = \chi_\sigma(\omega) + \frac{K_{SP} + i\lambda\omega}{K_{SP}^2 + (\lambda\omega)^2}, \tag{40}$$

where the first term is the susceptibility of the binary-filtered output of the continuous model and the second term is the (low-pass) susceptibility of the linear dynamics $\hat{X}(t)$. Indeed, when comparing the susceptibility from Eq. (40) to the original one (see Fig. 16), we see that the passive dynamics ac-

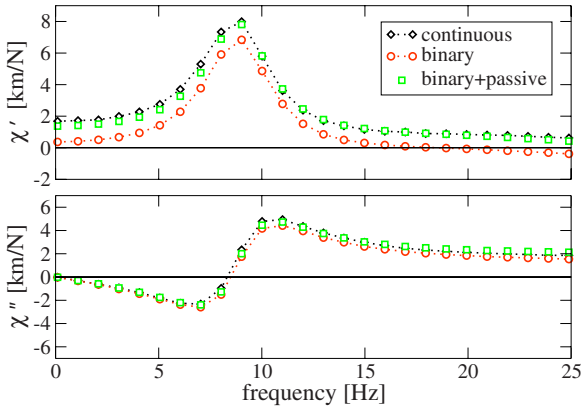

FIG. 16. (Color online) Real and imaginary part of the susceptibility of the continuous hair bundle model with respect to a sinusoidal driving force of amplitude 1 pN [diamonds and dotted line: continuous dynamics, circles and dotted line: binary-filtered dynamics, and squares: the sum of the susceptibilities of the binary dynamics and a passive dynamics according to the differential equation $\lambda\dot{\hat{X}}=-K_{SP}\hat{X}+F(t)+\eta_X(t)$].

counts for most of the small differences between the continuous and binary-filtered data. Also it becomes clear that for the parameter set chosen the correction to the real part is much larger than that to the imaginary part of the susceptibility because for typical frequencies below 10 Hz K_{SP} (the numerator of the real part's correction) is larger than $\omega\lambda$ (the numerator of the imaginary part) at least by a factor of 3.

B. Limitations of the two-state theory

The two-state theory describes the spontaneous power spectrum as well as the susceptibility with respect to a sinusoidal stimulus in a qualitative manner for the four parameter sets we considered in the previous section. Its main restriction for quantitative results lies in the finite time-scale separation of the dynamical variables which we neglected in our analytical approach. Peaks in the power spectrum occur generally at a higher frequency than found in the continuous hair bundle model. Since the integrated power of the spectrum is the same for the two-state and continuous hair bundle models, the peak height is therefore lower in the two-state model. Also the spectral features of the susceptibility such as the maximum in the real part and the zero in the imaginary part are shifted to higher frequencies in the two-state model. Furthermore, the absolute value of the susceptibility is increased at high driving frequencies. The maximum of the imaginary part is less pronounced compared to the minimum in the two-state theory. Those effects are mainly due to the adiabatic elimination of the fast variable by the approximation of a perfect time-scale separation.

One may ask how much of the difference can be accounted for by a simple rescaling of time. We consider the operation point of the hair bundle, $F_{max}=50.3$ pN, $S=0.65$. We rescale the frequency such that the peak frequency of the analytically obtained power spectrum matches the peak frequency of the power spectrum of the continuous hair bundle

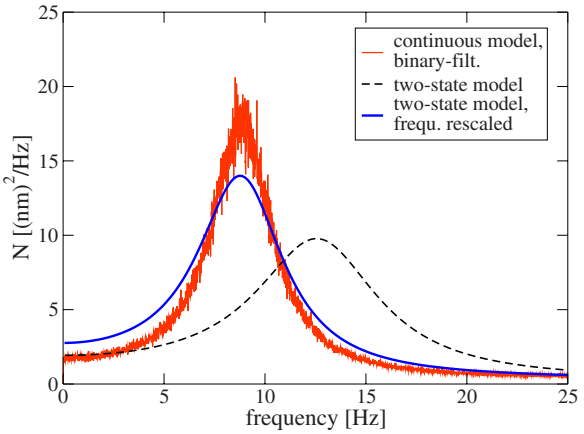

FIG. 17. (Color online) Frequency rescaling of the analytical power spectrum ($\zeta=0.698$) to match the simulation results for the operation point $F_{max}=50.3$ pN, $S=0.65$.

model. The characteristic frequency of the power spectrum in the two-state theory and in the continuous model is found at about 12.6 and 8.8 Hz, respectively, yielding a factor of rescaling $\zeta=8.8/12.6=0.698$. Such a rescaling can be also motivated by considering the natural frequency of a piecewise linear FN model for a *finite* time-scale separation [15]. The power spectrum $N(\omega)$ as a density rescales according to

$$\bar{N}(\omega')=N(\omega'\zeta^{-1})\zeta^{-1}, \tag{41}$$

whereas the amplitude of the susceptibility is not rescaled. Rescaling the frequency, the power spectrum of the two-state theory and simulation of the continuous hair bundle model are in reasonable agreement (cf. Fig. 17). Slight quantitative disagreement remains as the peak height is reduced by about 20% and the width of the peak is broader; the zero-frequency component is increased for the analytical power spectrum.

In the susceptibility (cf. Fig. 18) some effects remain that cannot be accounted for by a rescaling of the frequency. The peak of the real part and the zero of the imaginary part of the

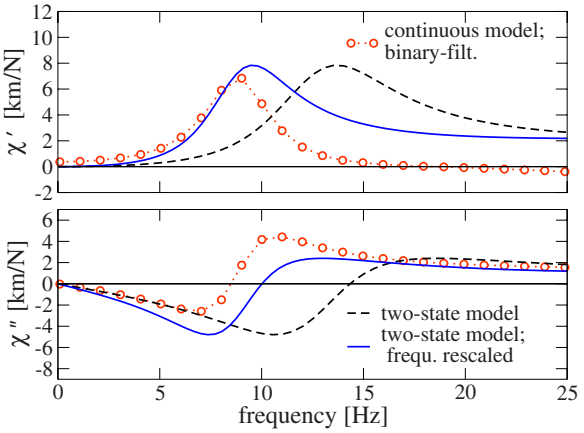

FIG. 18. (Color online) Frequency rescaling of the analytical susceptibility ($\zeta=0.698$) to match the simulation results for the operation point $F_{max}=50.3$ pN, $S=0.65$.

susceptibility remain offset compared to the simulation result to a higher frequency. The negative dip of the imaginary part is more, and its maximum less pronounced in the two-state theory compared to the continuous model.

C. Applications of the two-state theory

The two-state theory for the hair bundle describes the mechanical hair bundle dynamics approximately as we discussed before. The two-state model might provide a good description for the transduction current in the stereocilia. The large amplitude switches of the hair bundle position are related to the dynamics of opening and closure of transduction channels. Therefore the two-state theory could describe the transmitted signal upon hair bundle deflection during mechanoelectrical transduction.

Our theory simplifies the description of the hair bundle dynamics from a two-dimensional model to a one-dimensional two-state model. A realistic picture of the active process in hearing in vertebrates requires the study of coupled hair cells. Our simplified model could therefore prove useful to the study of huge collections of coupled hair bundles. This remains an interesting task for future studies.

APPENDIX A: BIFURCATION LINES FOR THE TWO-STATE MODEL

Bifurcations in the two-state hair bundle model correspond to bifurcations in the piecewise linear FN system. The points (F^*_{max}, S^*) in the (F_{max}, S) plane at which bifurcations occur satisfy one of the following equations which correspond to the intersection of the two nullclines of the piecewise linear FN system in the minimum or maximum point of $g(x)$, respectively:

$$y_m = g(x_m) = Bx_m + y_0, \tag{A1}$$

TABLE I. Parameter values for the simulation of the continuous hair bundle model. F_{max} and S are the free parameters of the continuous hair bundle model.

λ	2.8 μNs/m	λ_a	10 μNs/m	N	50
K_{GS}	750 μN/m	K_{SP}	600 μN/m	D	61 nm
C_M	0.1 mM	T	300 K	ΔG	10 k_BT
F_0	1 pN	τ_c	1 ms		

$$y_M = g(x_M) = Bx_M + y_0. \tag{A2}$$

The parameters x_m, y_m, x_M, y_M, and B depend on the product of parameters $F_{max}S$ through the parameter β, whereas y_0 depends on both β and S. Equations (A1) and (A2) can therefore be rearranged such that we obtain a parametrization of the bifurcation lines in terms of β,

$$S^* = \frac{\beta}{1-\beta}(Bx_m - y_m), \quad F^*_{max} = \frac{\beta D K_{GS}}{S^*}, \tag{A3}$$

$$S^* = \frac{\beta}{1-\beta}(Bx_M - y_M), \quad F^*_{max} = \frac{\beta D K_{GS}}{S^*}. \tag{A4}$$

Varying β gives the bifurcation lines shown in Fig. 11.

APPENDIX B: SIMULATION PARAMETERS

Stochastic simulations of the continuous hair bundle model were performed with a time step of 0.2 ms. To calculate power spectra and susceptibilities an ensemble of 200 trajectories of 105 s duration was simulated and averaged over. The parameters of the continuous hair bundle model (see Table I) were adopted from [7], except that we set τ used in that paper to zero, and that the gating swing D here corresponds to d/γ in that paper's notation.

[1] A. J. Hudspeth, in *Principles of Neural Science*, edited by E. R. Kandel, J. H. Schwartz, and T. M. Jessel (McGraw-Hill, New York, 2000), pp. 614–624.

[2] P. Martin, A. J. Hudspeth, and F. Jülicher, Proc. Natl. Acad. Sci. U.S.A. **98**, 14380 (2001).

[3] P. Martin and A. J. Hudspeth, Proc. Natl. Acad. Sci. U.S.A. **96**, 14306 (1999).

[4] P. Martin and A. J. Hudspeth, Proc. Natl. Acad. Sci. U.S.A. **98**, 14386 (2001).

[5] S. Camalet, T. Duke, F. Jülicher, and J. Prost, Proc. Natl. Acad. Sci. U.S.A. **97**, 3183 (2000).

[6] Y. Choe, M. Magnasco, and A. J. Hudspeth, Proc. Natl. Acad. Sci. U.S.A. **95**, 15321 (1998).

[7] B. Nadrowski, P. Martin, and F. Jülicher, Proc. Natl. Acad. Sci. U.S.A. **101**, 12195 (2004).

[8] J.-Y. Tinevez, F. Jülicher, and P. Martin, Biophys. J. **93**, 4053 (2007).

[9] B. Lindner, J. García-Ojalvo, A. Neiman, and L. Schimansky-Geier, Phys. Rep. **392**, 321 (2004).

[10] B. Lindner and L. Schimansky-Geier, Phys. Rev. E **61**, 6103 (2000).

[11] L. Meinhold and L. Schimansky-Geier, Phys. Rev. E **66**, 050901(R) (2002).

[12] A. J. Hudspeth and P. G. Gillespie, Neuron **12**, 1 (1994).

[13] R. L. Stratonovich, *Topics in the Theory of Random Noise* (Gordon and Breach, New York, 1967).

[14] M. Abramowitz and I. A. Stegun, *Handbook of Mathematical Functions* (Dover, New York, 1970).

[15] D. Clausznitzer, Diploma thesis, Technische Universität Dresden, Germany, 2007 (unpublished).

[16] For a pronounced time-scale separation also the typical slope of $f(x)$ as well as B should not be much bigger than one. For the parameter region explored in this paper this is the case.